Supplementary Information (SI) for Journal of Materials Chemistry C.
This journal is © The Royal Society of Chemistry 2025

Supporting Information for

Enhanced Specific Detectivity of ternary Near−Infrared Organic Photodetector with ZnO/PDIN Double−Electron Transport Layer for health monitoring

Honglin Wang[a,b], Minghao Wang[a,b], Jingchong Liang[a,b], Dawei Yan[a,c], Linghai Xie[d] , Xiaoya Hou[a,b,*], and Jie Zhang[a,b]

[a] *School of Mechanical Engineering, Jiangnan University, No.1800, Lihu Avenue, Wuxi City, Jiangsu 214122, P.R. China.*

[b] *Jiangsu Key Laboratory of Advanced Food Manufacturing Equipment and Technology (Jiangnan University).*

[c] *School of Internet of Things Engineering, Jiangnan University, No.1800, Lihu Avenue, Wuxi City, Jiangsu 214122, P.R. China.*

[d] *Nanjing University of Posts and Telecommunications, Nanjing City, Jiangsu 210023, P.R. China.*

E-mail: xiaoyahou@jiangnan.edu.cn

1. Responsivity and Specific detectivity characteristics

Responsivity in OPDs can be measured by the following equation[1]

$$R = EQE\frac{q\lambda}{hc} = \frac{EQE \times \lambda}{1240} \tag{S1}$$

where q is elementary charge (1.6×10^{-19}C), λ is the wavelength of incident light, h is Planck's constant, and c is the speed of light. The specific detection rate is obtained by equations 2 and 3. [2,3]

$$D_{shot}^{*} = \frac{R}{\sqrt{2qJ_D}} \tag{S2}$$

$$D^{*} = \frac{\sqrt{AB}}{NEP} = \frac{\sqrt{AB} \times R}{i_n} \tag{S3}$$

Formula 2 represents the D^* when the noise of the device is mainly composed of shot noise. Formula 3 is the specific detection rate obtained from the noise current, which can prevent the D^* from being overestimated. The difference between the values obtained from the two formulas can reflect the degree of influence of shot noise affected by dark current on devices performance.

2 Supporting Figs

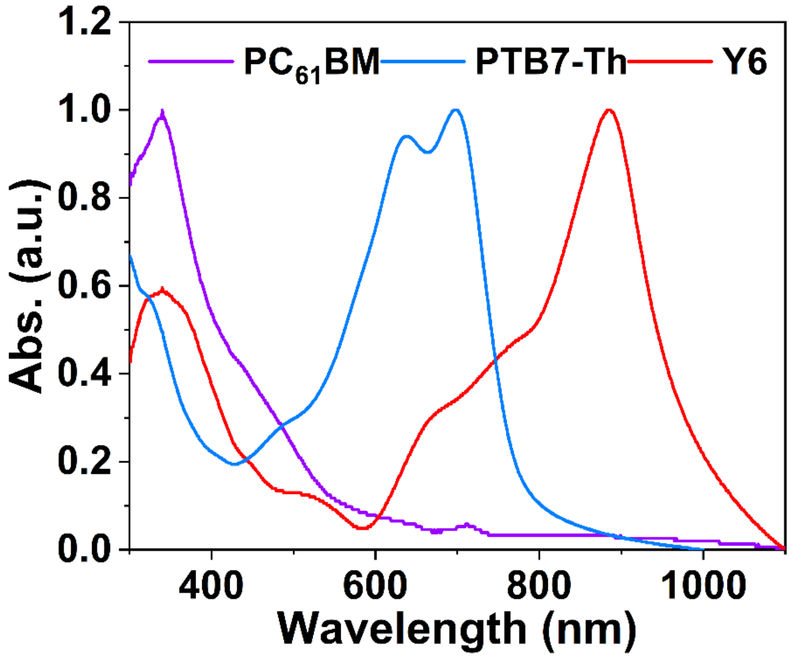

Fig. S1. Normalized absorption spectra of three materials, $PC_{61}BM$, PTB7-Th, Y6.

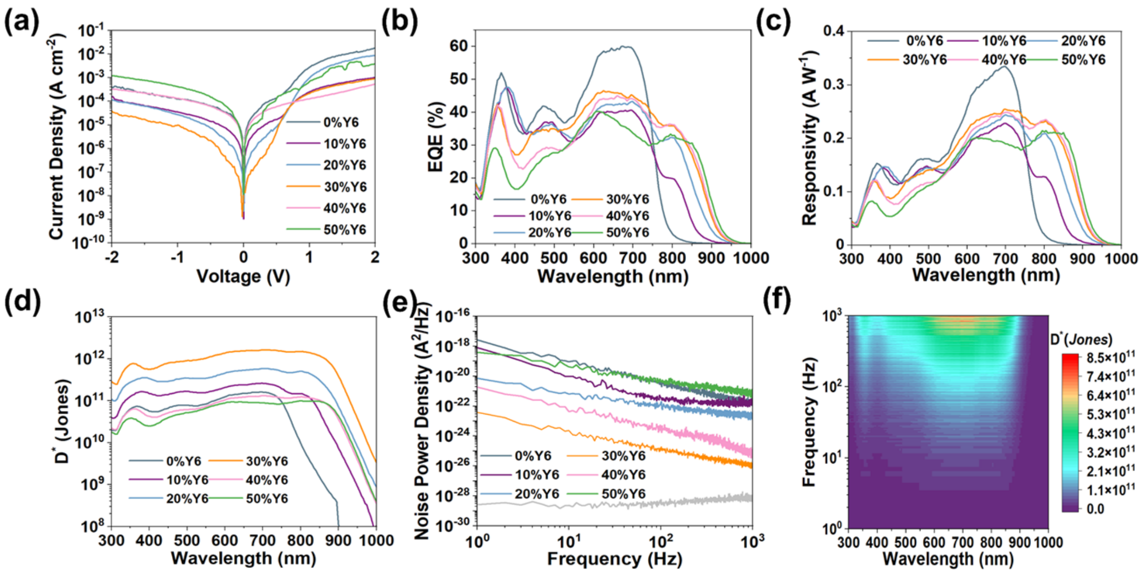

Fig. S2 (a) The dark J-V curves, (b) EQE curves, (c) Responsivity curves, (d) Specific detectivity curves obtained from J_D, (e) Noise spectral densities, and (f) NIR- specific detectivity spectra obtained from the noise current for OPDs with different Y6 weight fractions.

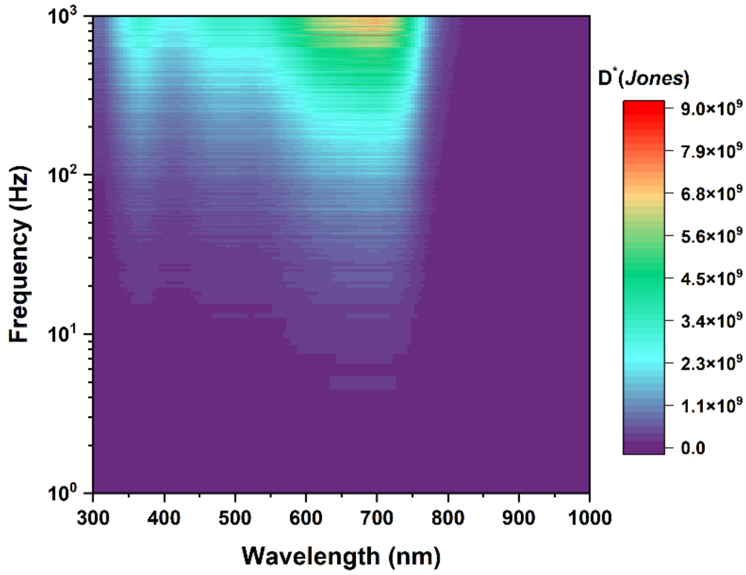

Fig. S3. D^* spectra of binary device from noise.

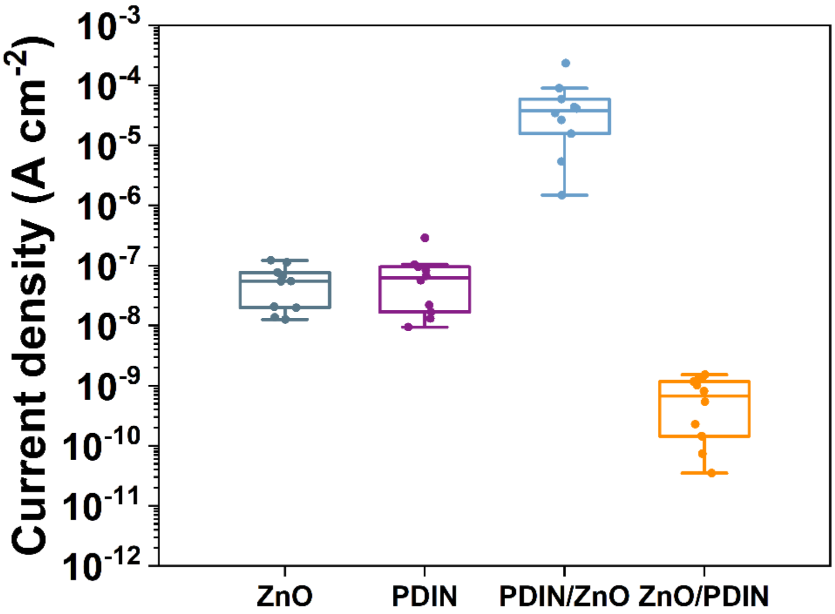

Fig. S4. Dark current box plots of 10 devices fabricated separately under different ETLs.

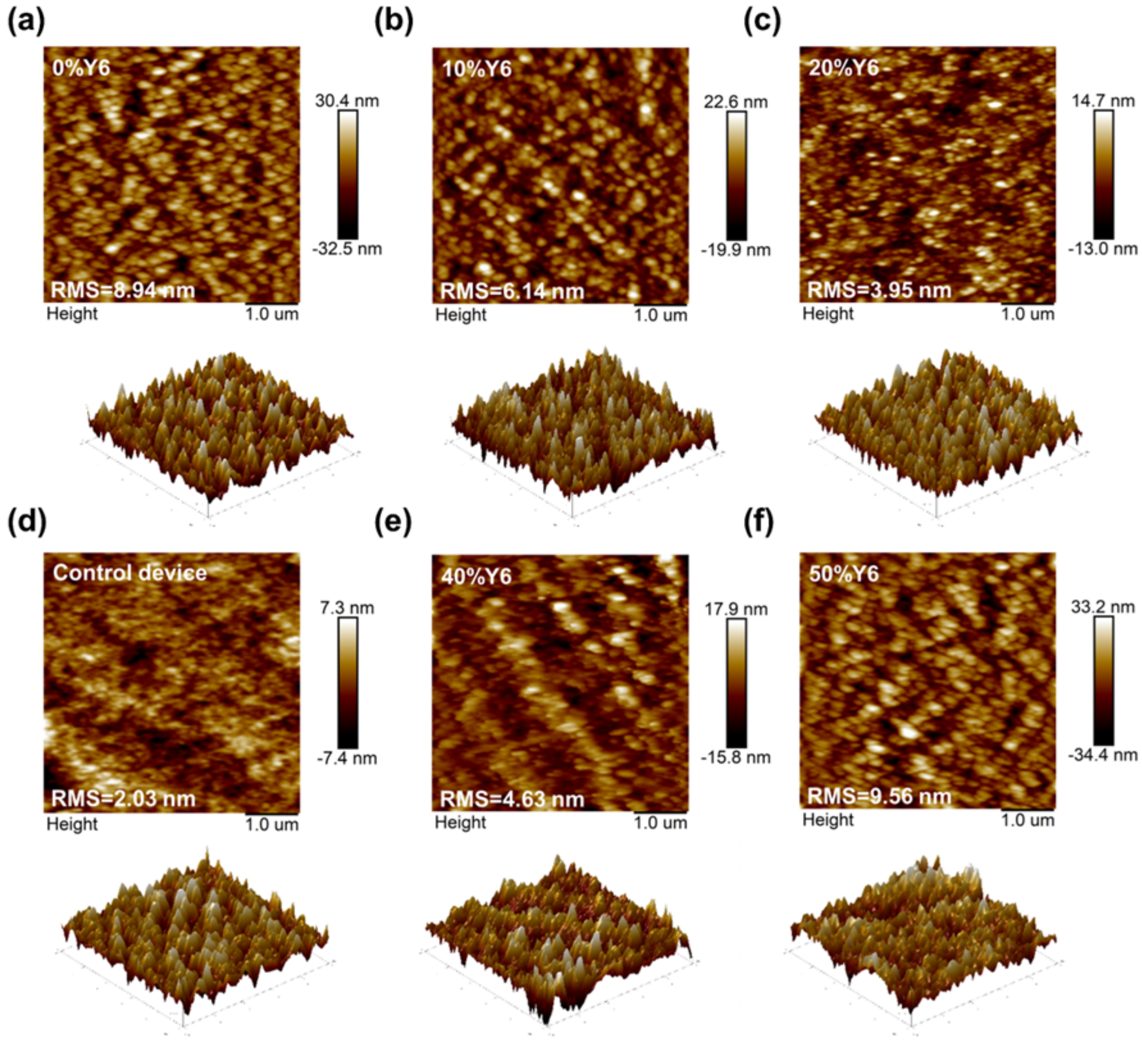

Fig. S5. AFM height images (5 × 5 μm) and 3D AFM diagrams of the active layers on (a) 0%Y6, (b) 10%Y6, (c) 20%, (d) 30%Y6, (e) 40%Y6, and (f) 50%Y6.

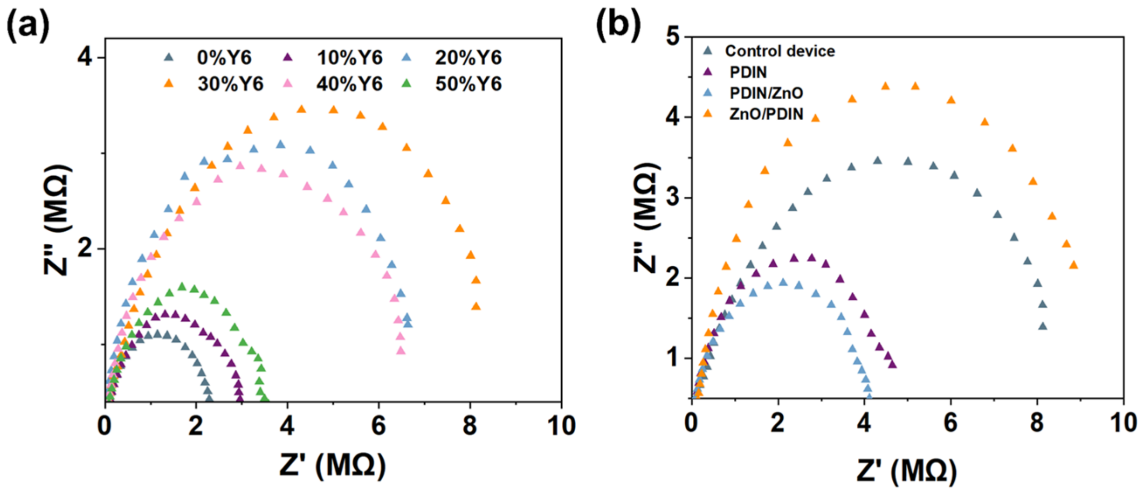

Fig. S6. Impedance spectra of OPDs with (a) different Y6 weight fractions and (b) different ETLs.

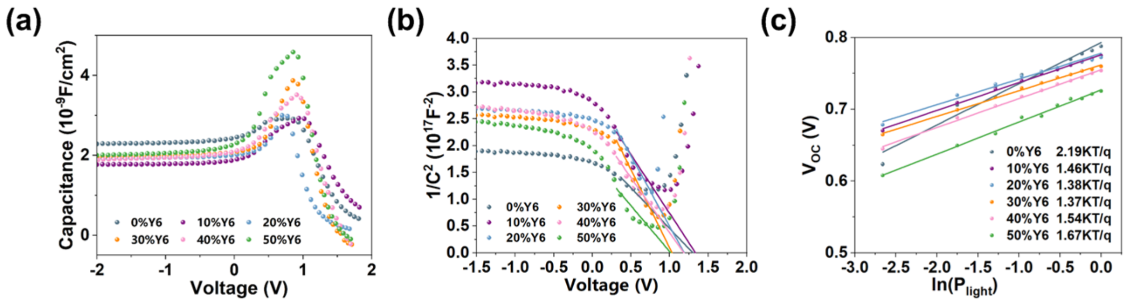

Fig. S7. (a) Capacitance-Voltage curves, (b) Mott Schottky curves, and (c) Dependence of the open-circuit voltage on light intensity of OPDs with different Y6 weight fractions.

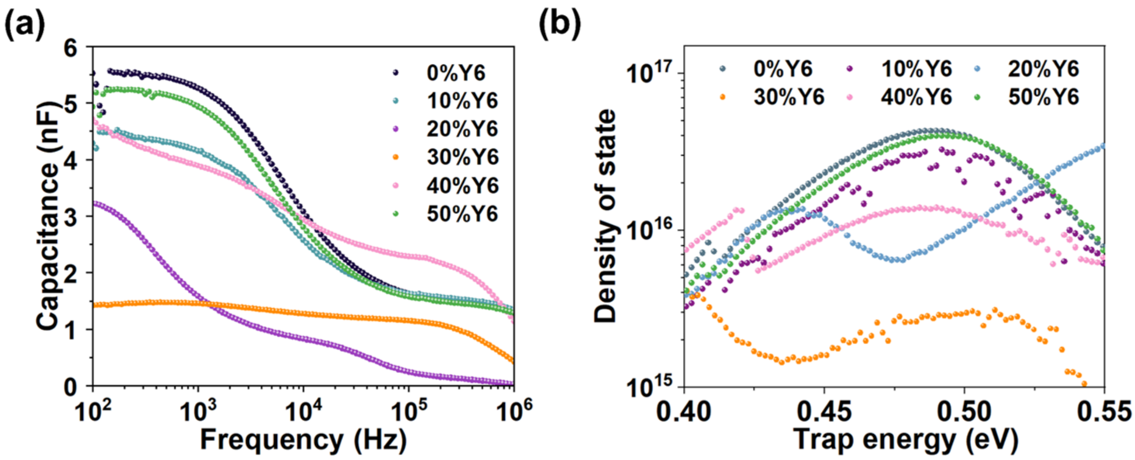

Fig. S8. (a-b) Capacitance-Frequency curves and trap density of state curves of OPDs with different Y6 weight fractions.

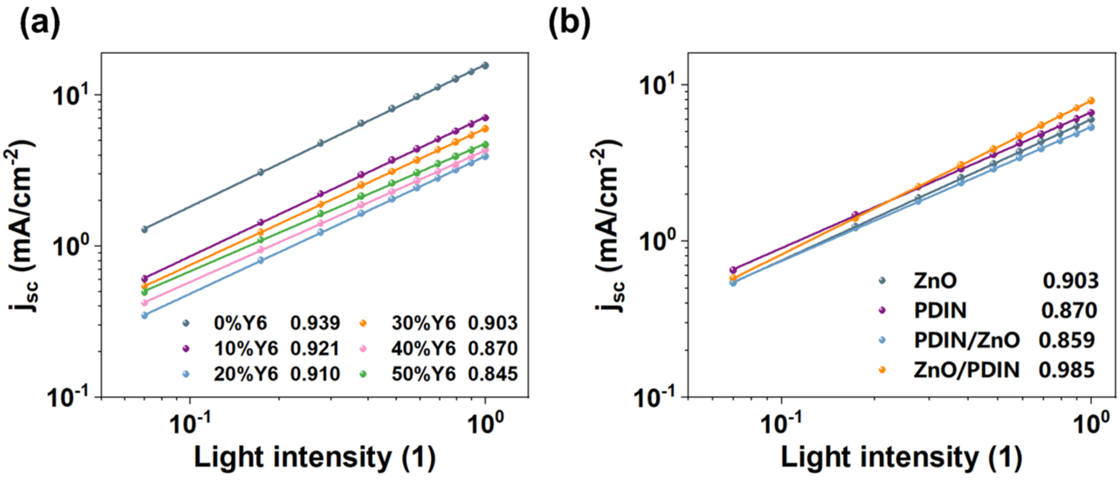

Fig. S9. (a-b) Dependence of short-circuit current on light intensity of OPDs with different Y6 weight fractions and ETLs.

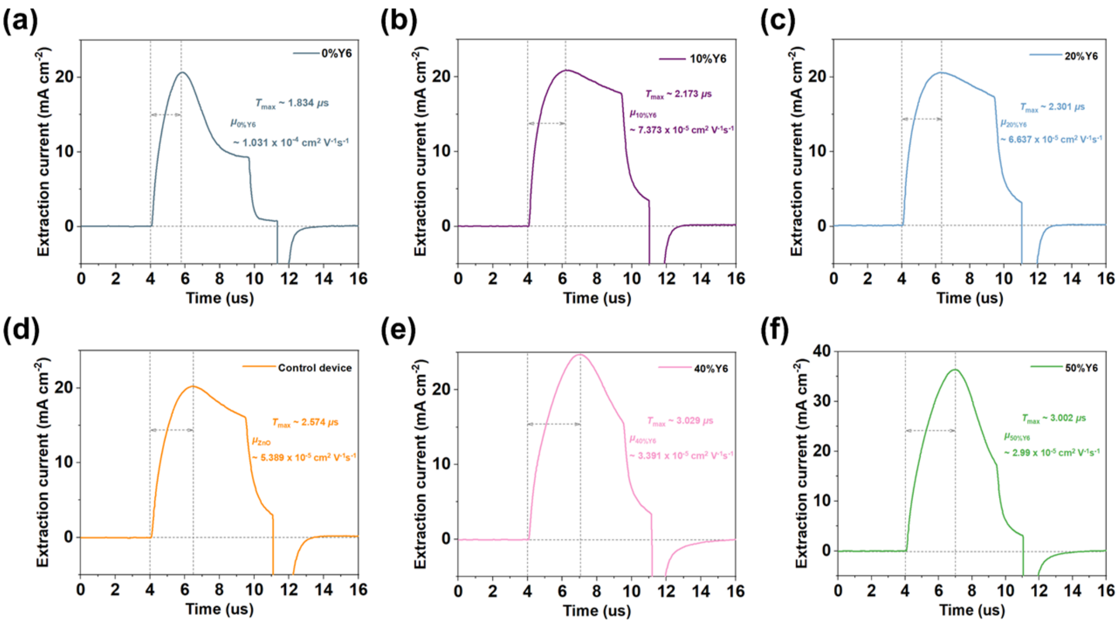

Fig. S10. (a-f) Carrier mobility of OPDs with different Y6 weight fractions.

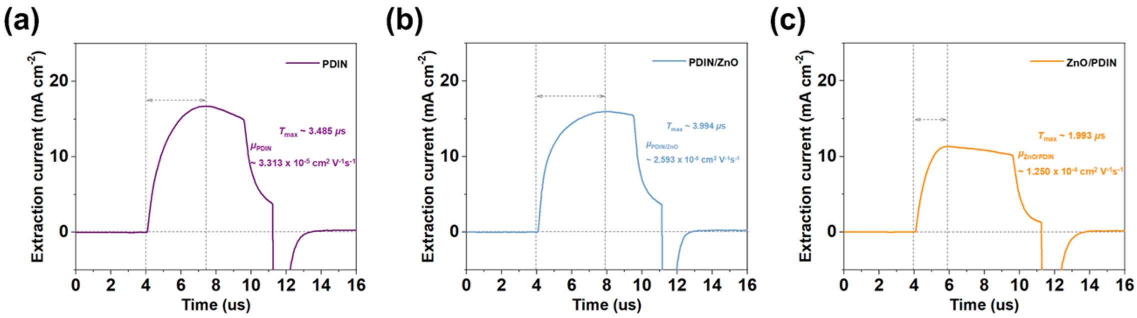

Fig. S11. (a-c) The carrier mobility of OPDs with different ETLs.

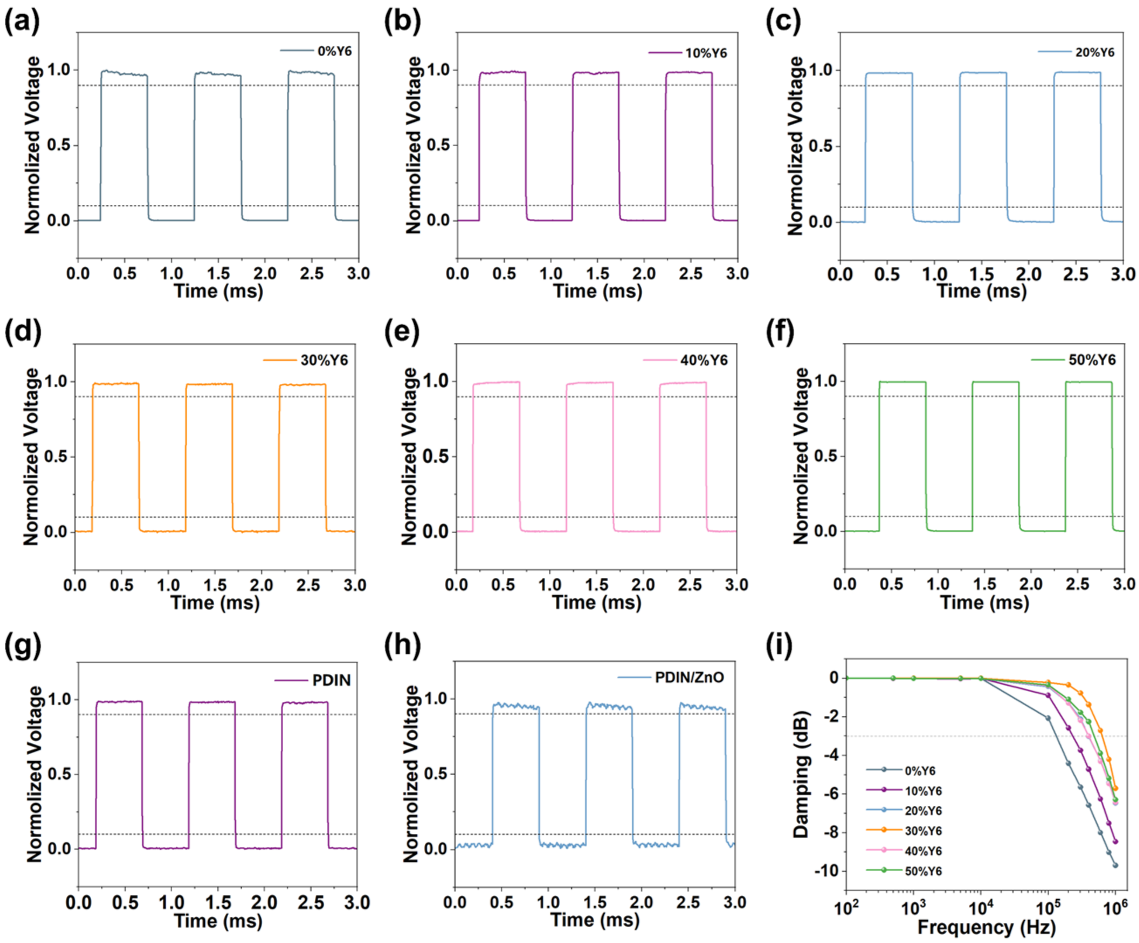

Fig. S12. (a-h) The response speed of OPDs with different Y6 weight fractions and ETLs. (i) -3dB cutoff frequency of OPDs with different Y6 weight fractions.

Fig. S13. Oximetry monitoring using a commercial oximeter (model: KE-6007)

3 Supporting Tables

Table S1. Main performance parameters of OPDs with different Y6 weight fractions.

Devices	J_D (A cm^{-2})	EQE % /R		D^*_{shot} (Jones)		D^* (Jones)	
	-0.1 V	650 nm	808 nm	650 nm	808 nm	650 nm	808 nm
0% Y6	1.4×10^{-5}	59%/0.31	2%/0.02	1.5×10^{11}	6.3×10^{9}	4.6×10^{9}	1.7×10^{8}
10% Y6	2.4×10^{-6}	40%/0.12	18%/0.12	2.4×10^{11}	1.4×10^{11}	5.5×10^{11}	3.2×10^{11}
20% Y6	5.5×10^{-7}	42%/0.22	31%/0.20	5.3×10^{11}	4.8×10^{11}	5.8×10^{11}	5.3×10^{11}
30% Y6	7.7×10^{-8}	45%/0.24	34%/0.23	1.5×10^{12}	1.4×10^{12}	6.3×10^{11}	5.9×10^{11}
40% Y6	1.1×10^{-5}	44%/0.23	35%/0.23	1.2×10^{11}	1.2×10^{11}	6.0×10^{11}	6.0×10^{11}
50% Y6	1.5×10^{-5}	38%/0.20	32%/0.21	9.2×10^{10}	9.7×10^{10}	5.2×10^{11}	5.5×10^{11}

Table S2. Main performance parameters of OPDs with different ETLs.

ETL	J_D (A cm^{-2})	EQE %/R		D^*_{shot} (Jones)		D^* (Jones)	
	-0.1 V	650 nm	808 nm	650 nm	808 nm	650 nm	808 nm
ZnO （control device）	7.7×10^{-8}	45%/0.24	34%/0.23	1.5×10^{12}	1.4×10^{12}	6.3×10^{11}	5.9×10^{11}
PDIN	2.9×10^{-7}	43%/0.23	36%/0.24	7.5×10^{11}	7.8×10^{11}	6.0×10^{11}	6.2×10^{11}
PDIN/ZnO	2.6×10^{-5}	34%/0.18	28%/0.18	6.2×10^{10}	6.2×10^{10}	4.7×10^{11}	4.8×10^{11}
ZnO/PDIN	1.4×10^{-10}	49%/0.26	42%/0.27	3.8×10^{13}	4.0×10^{13}	1.2×10^{13}	1.3×10^{13}

Table S3. Trap density and depletion width of OPDs with different Y6 weight fractions.

Devices	V_{bi}	N_A (cm^{-3})	W	n KT/q
0% Y6	1.27 V	6.57×10^{16}	95 nm	2.19 KT/q
10% Y6	1.31 V	3.36×10^{16}	114 nm	1.46 KT/q
20% Y6	1.15 V	2.81×10^{16}	115 nm	1.38 KT/q
30% Y6	1.00 V	2.53×10^{16}	117 nm	1.37 KT/q
40% Y6	1.16 V	3.59×10^{16}	104 nm	1.54 KT/q
50% Y6	0.99 V	4.38×10^{16}	86 nm	1.67 KT/q

Table S4. Trap state density of OPDs with different Y6 weight fractions and different ETLs.

Devices (Y6 weight fractions @ ETL)	DOS @ 0.5 eV ($cm^2 V^{-1} S^{-1}$)
0% @ ZnO	3.90×10^{16}
10% @ ZnO	2.99×10^{16}
20% @ ZnO	1.01×10^{16}
30% @ ZnO	2.91×10^{15}
40% @ ZnO	1.24×10^{16}
50% @ ZnO	3.84×10^{16}
30% @ PDIN	5.64×10^{15}
30% @ PDIN/ZnO	9.04×10^{15}
30% @ ZnO/PDIN	2.06×10^{15}

Table S5. Bimolecular recombination coefficients, carrier mobility, and charge transfer time of OPDs.

Devices	α	T_{max} (μs)	μ ($cm^2 V^{-1} S^{-1}$)	$\tau_{e,h}$ (μs)
0% Y6	0.939	1.834	1.031×10^{-4}	3.630
10% Y6	0.921	2.173	7.373×10^{-5}	4.920
20% Y6	0.910	2.301	6.637×10^{-5}	6.226
30% Y6	0.903	2.574	5.389×10^{-5}	8.822
40% Y6	0.870	3.029	3.391×10^{-5}	12.082
50% Y6	0.845	3.002	2.990×10^{-5}	16.055

Table S6. Response speed and -3dB bandwidth of OPDs with different Y6 weight fractions and ETLs.

Devices (Y6 weight fraction @ ETL)	Rise time (μs)	Fall time (μs)	Response speed (μs)	-3dB (MHz)
0% @ ZnO	3.594	8.803	11.677	134
10% @ ZnO	3.326	6.575	9.901	236
20% @ ZnO	2.158	4.628	8.789	398
30% @ ZnO	1.292	2.990	4.282	625
40% @ ZnO	1.121	3.306	4.427	402
50% @ ZnO	1.173	4.967	6.140	467
30% @ PDIN	2.478	2.590	5.068	528
30% @ PDIN/ZnO	4.526	4.276	8.902	390
30% @ ZnO/PDIN	0.534	1.940	2.474	1000

Table S7. Comparison of performances of OPDs in this work with others.

Active Layer	ETL	J_D (A cm^{-2})	R (A/W)	D^*_{shot} (Jones)	D^* (Jones)	-3dB	Ref
PM7: D5: Y12	ZnO	3.60×10^{-9}	0.400	3.20×10^{13}	—	82.9 kHZ	[4]
PTB7-Th: $PC_{71}BM$: COTIC-4F	PEI-Zn	3.80×10^{-10}	0.530	4.80×10^{13}	4.73×10^{11}	1 MHZ	[5]
PIPCP: $PC_{61}BM$	ZnO	—	0.144	—	1.34×10^{11}	1 kHZ	[6]
PF3:IT-4F	ZnO	5.60×10^{-9}	0.310	3.39×10^{13}	7.40×10^{12}	63.4 kHZ	[7]
TQ-3T: IEICO-4F	ZnO	2.30×10^{-6}	0.050	—	1.03×10^{10}	470 kHZ	[8]
PM6: Y6	PDINN	7.10×10^{-10}	0.504	3.35×10^{13}	—	176 kHZ	[9]
PTB7-Th: $PC_{61}BM$: Y6	ZnO/PDIN	1.40×10^{-10}	0.270	4.03×10^{13}	2.14×10^{13}	1 MHZ	This work

4 Calculation of oximetry data

Table S1. Extraction of PPG seven groups of arterial pulse signals (650 nm light).

Extraction of PPG signals in 650 nm light					
AC+DC1	154.5	DC1	147.8	Ratio 1	0.045331529
AC+DC2	155.5	DC2	148.8	Ratio 2	0.045026882
AC+DC3	156.1	DC3	148.9	Ratio 3	0.0483546
AC+DC4	157.2	DC4	150.6	Ratio 4	0.043824701
AC+DC5	156.3	DC5	149.5	Ratio 5	0.04548495
AC+DC6	156.2	DC6	149.4	Ratio 6	0.045515395
AC+DC7	157.1	DC7	149.7	Ratio 7	0.049432198

Table S2. Extraction of PPG seven groups of arterial pulse signals (808 nm light).

Extraction of PPG signals in 808 nm light					
AC+DC1	140	DC1	130	Ratio 1	0.076923077
AC+DC2	141.5	DC2	131.8	Ratio 2	0.073596358
AC+DC3	143.2	DC3	133	Ratio 3	0.076691729
AC+DC4	142.5	DC4	132.8	Ratio 4	0.073042169
AC+DC5	141.9	DC5	131.8	Ratio 5	0.076631259
AC+DC6	141.4	DC6	131.7	Ratio 6	0.07365224
AC+DC7	141.7	DC7	131.1	Ratio 7	0.08085431

Table S3. Calculation of blood oxygen data.

Modulation ratio		SPO_2
ROS1	0.589309878	0.96057
ROS2	0.611808558	0.95504
ROS3	0.630506064	0.95045
ROS4	0.599991785	0.95794
ROS5	0.593556078	0.95952
ROS6	0.617977063	0.95353
ROS7	0.611373691	0.95515

Supporting References

1 X. Hou, K. Zhang, J. Li, J. Liang, W. Li, D. Yan, L. Liu, J. Zhang, *J. Mater. Chem. C*, 2023, **11**, 9229-9237.

2 L. Lv, J. Yu, X. Sui, J. Wu, X. Dong, G. Lu, X. Liu, A. Peng, H. Huang, *J. Mater. Chem. C*, 2019, **7**, 5739-5747.

3 S. Xing, J. Kublitski, C. Hänisch, L.C. Winkler, T. Li, H. Kleemann, J. Benduhn, K. Leo, *Adv. Sci.,* 2022, **9**, 2105113.

4 Z. Du, H.M. Luong, S. Sabury, A.L. Jones, Z. Zhu, P. Panoy, S. Chae, A. Yi, H.J. Kim, S. Xiao, V.V. Brus, G.N.M. Reddy, J.R. Reynolds, T.-Q. Nguyen, *Adv. Mater.*, 2024, **36**, 2310478.

5 Z. Lou, J. Tao, B. Wei, X. Jiang, S. Cheng, Z. Wang, C. Qin, R. Liang, H. Guo, L. Zhu, P. Müller‐Buschbaum, H. Cheng, X. Xu, *Adv. Sci.*, 2023, **10**, 2304174.

6 S. Park, K. Fukuda, M. Wang, C. Lee, T. Yokota, H. Jin, H. Jinno, H. Kimura, P. Zalar, N. Matsuhisa, S. Umezu, G.C. Bazan, T. Someya, *Adv. Mater.*, 2018, **30**, 1802359.

7 B. Park, J. Jung, D. Lim, H. Lee, S. Park, M. Kyeong, S. Ko, S.H. Eom, S. Lee, C. Lee, S.C. Yoon, Adv. *Funct. Mater.*, 2022, **32**, 2108026.

8 P. Jacoutot, A.D. Scaccabarozzi, D. Nodari, J. Panidi, Z. Qiao, A. Schiza, A.D. Nega, A. Dimitrakopoulou-Strauss, V.G. Gregoriou, M. Heeney, C.L. Chochos, A.A. Bakulin, N. Gasparini, *Sci. Adv.*, 2023, **9**, eadh2694.

9 Z. Yang, Efficient Noise Suppression via Controlling the Optical Cavity in Near-Infrared Organic Photoplethysmography Sensors, *J. Mater. Chem. C*, 2024, **12**, 3261-3271.